Repulsion and Metabolic Switches in the Collective Behavior of Bacterial Colonies

A. Sekowska,[†] J.-B. Masson,[†] A. Celani,[†] A. Danchin,[‡] and M. Vergassola[†*]
[†]Institut Pasteur Unit for In Silico Genetics, and [‡]Institut Pasteur Unit for Genetics of Bacterial Genomes, Centre National de la Recherche Scientifique URA 2171, Paris, France

ABSTRACT Bacteria inoculated on surfaces create colonies that spread out, forming patterns shaped by their mutual interactions. Here, by a combination of experiments and modeling, we address two striking phenomena observed when colonies spread out circularly, without dendritic instabilities. First, the velocity of spreading is generically found to decrease as levels of nutrients initially deposited on the surface increase. We demonstrate that the slowdown is due to phenomena of differentiation, leading to the coexistence of bacteria in different states of motility and we model their dynamics. Second, colonies spreading out from different inocula on the same surface are observed to merge or repel (halting at a finite distance), depending on experimental conditions. We identify the parameters that determine the fate of merging versus repulsion, and predict the profile of arrest in the cases of repulsion.

INTRODUCTION

Bacteria are often found in the form of organized colonies living on solid surfaces or inorganic substrates such as prostheses or medical devices. These multicellular aggregates feature a breadth of collective strategies to effectively respond to changing, possibly hostile conditions. This is accomplished through a variety of intercellular communication mechanisms, featuring both direct and indirect interactions, via extracellular polymer matrices and the excretion of signaling molecules. The term ''sociomicrobiology'' has been coined to describe the emerging discipline addressing communication among bacteria and their collective behavior.

The growth of bacterial colonies on a dish possibly constitutes the simplest instance of nontrivial collective behavior. Depending on experimental conditions, colonies develop dendritic ramifications and other complex patterns (1–4) or expand radially (5). Even for the latter case, important dynamical processes remain to be quantitatively understood.

First, front velocities are found to depend on environmental conditions such as temperature, hardness of the surface, humidity, etc. In particular, it is observed experimentally that the velocity decreases with increasing values of the initial concentration of nutrients on the plate. This is quite puzzling, as standard models, such as the Fisher-Kolmogorov (6), would predict constant velocities.

Second, nontrivial interactions take place when several inocula of the same culture are spotted on the plate and their fronts approach each other. Depending on experimental conditions, colonies can either merge into a single one (Fig. 1 *b*) or halt their progression (Fig. 1, *a*, *c*, and *d*). In the latter case, regions among the various colonies are nearly devoid of bacteria and remain so throughout the observation time.

These two phenomena (slowdown of the front velocity and repulsion among approaching subcolonies) are highly reproducible and generic. We observed them with bacterial species as different as *Bacillus subtilis*, *Pseudoalteromonas haloplanktis*, *Salmonella typhimurium*, and *Escherichia coli*, hinting at a general physical/chemical constraint or/and common genetic features conserved in different bacterial clades. Furthermore, the same effects are observed under different conditions of growth (5). Previous theoretical models to explain the slowdown (7) specifically considered the case of the setup in Budrene and Berg (8). The explanation hinges on the fact that bacteria are chemotactically sensitive to the excreted substance (aspartate) and not to the original nutrients deposited on the plate (succinate). Conversely here, we employ the sugar glucose as a source of nutrients, which is a strong chemoattractant (9), and still observe the slowdown. As for the repulsion effect, it is unknown what the conditions are that control whether repulsion or merging will take place. It is of particular biological interest to understand the role of nutrients, intercellular signaling, and switches in the metabolic programs during the space-time development of the colony and the relation of those phenomena to more elaborated patterns. Our aim here is to provide an answer to these questions by the concerted interplay of experiments and theoretical models.

MATERIALS

Bacterial strains and culture conditions

Salmonella enterica subsp. enterica serovar *typhimurium* LT-2 (10), *E. coli* MG1655 (11), *P. haloplanktis* TAC125 (12), and *B. subtilis* 168 (13) strains were used in all experiments. *E. coli* and *S. typhimurium* were grown in 18 g/L nutrient broth (NB) from Difco (Franklin Lakes, NJ), supplemented with 0.4% glucose or in M63 medium (14) or in medium A (described in the

Submitted November 14, 2008, and accepted for publication April 1, 2009.

*Correspondence: massimo@pasteur.fr

Editor: Herbert Levine.

0006-3495/09/08/0688/11 $2.00

doi: 10.1016/j.bpj.2009.04.018

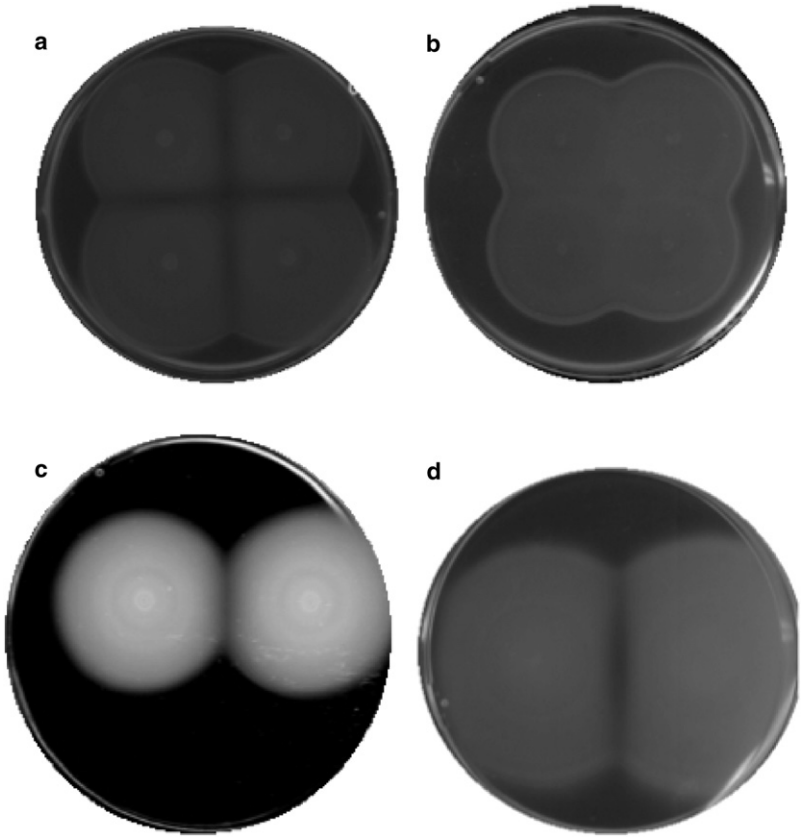

FIGURE 1 Repulsion versus merging of bacterial colonies. (*Upper row*) *S. typhimurium* at 30°C in medium A. (*a*) Repulsion with 0.4% glucose and 0.6% Eiken agar, after 24 h. (*b*) Merging with 0.05% glucose and 0.4% Eiken agar after 24 h. (*c*) Repulsion in *P. haloplanktis* at 15°C in rich medium with 0.3% Bacto-agar after three days. (*d*) Repulsion in *E. coli* at 30°C in medium A with 0.3% glucose after three days.

Supporting Material). For plate experiments, glucose was used instead of glycerol. *P. haloplanktis* was grown in a mineral medium described in Bozal (15) without $CaCl_2$ and instead with 2% NaCl, 0.1% tyrosine, and 0.4% gluconate. *B. subtilis* was grown in ED1 medium (see Supporting Material). Bacteria were grown at 37°C (*E. coli*, *S. typhimurium*, and *B. subtilis*) or 4°C (*P. haloplanktis*). The optical density (OD) of bacterial cultures was measured at 600 nm. Plates were prepared by the addition of 3 g/L Bacto agar, Agar Noble (Difco), or Eiken agar (Eiken Chemicals, Tokyo, Japan) to the medium. For *B. subtilis* plates prepared with either Bacto Agar or Agar Noble, 5×10^{-3}% SDS was added to the medium.

Enumeration of bacteria

Bacteria were counted by the agarase treatment. Briefly, 1 μL of solidified medium (0.3% agar) with bacteria was removed using a Hamilton syringe and injected into 950 μL of sterile 50 mM NaH_2PO_4 at pH 6. Fifty units of agarase (agarase from *Pseudomonas atlantica*, Sigma-Aldrich (St. Louis, MO) prepared in the same buffer at 1000 U/mL) were added to the Eppendorf tube, vortexed, and incubated for 40 min at 37°C. Bacteria were counted by serial dilution on plates.

Motility assays

Bacteria grown in the overnight cultures were diluted into the fresh medium at OD 0.1 and grown until the stationary growth phase. For the microscopic observations, 2 μL of the culture was inoculated directly in the center of the plate containing 20 mL of the medium. The plate was placed under the stereomicroscope on the heating stage (Tokai Hit, Shizuoka, Japan) maintaining a constant temperature during the observation, and within a custom-made culture chamber to avoid desiccation. For the comparative studies on minimal media, 10^4 bacteria were inoculated on a plate containing 10 mL of medium and the plates were incubated either in 23°C or 4°C incubator. For the observations on NB plates, different quantities of bacteria (10^4, 10^5, or 10^6 in 1 μL injected with the Hamilton syringe) were inoculated on plates containing 24 mL of NB medium and incubated at 37°C.

Quorum sensing assay

S. typhimurium was inoculated into 100 mL of NB medium at OD_{600nm} 0.1 and grown for 5 h at 37°C with 180 rpm agitation. The culture was centrifuged for 5 min at 5000 rpm at 4°C and the supernatant was passed through a 0.22-μm filter unit. Sterile supernatant was kept at 4°C until use. For plates used in motility tests, half of the original volume was replaced with supernatant and the assay was carried out as described above.

Glucose quantification

To measure glucose concentration, the QuantiChrom Glucose Assay Kit (BioAssay Systems, Research Triangle Park, NC) was employed. Samples of 12 μL were taken using a Hamilton syringe and used in the assay following the protocol. The diffusion coefficient of glucose was obtained by measuring its concentrations at different distances from the point of injection of a small drop.

Image acquisition and treatment

All the observations were made under the minimal magnification using a Stereomicroscope Discovery V8 equipped with an AxioCam MRm, Ver.3, and Axiovision software (Carl Zeiss, Oberkochen, Germany). For time-lapse acquisition, the images were taken every 5 min using the 500-ms exposition time for the camera. File-series were treated using ImageJ freeware (http://rsbweb.nih.gov/ij/).

QUANTITATIVE EXPERIMENTAL AND THEORETICAL ANALYSIS OF *S. TYPHIMURIUM* MOTILITY

Theoretical modeling

Classical models for the evolution of bacterial colonies are based on the following system of reaction-diffusion partial differential equations (see, e.g., (6)) for the density of bacteria $n(\boldsymbol{r},t)$ and nutrients $c(\boldsymbol{r},t)$:

$$\partial_t n + \boldsymbol{\nabla}\cdot(n\chi(c)\boldsymbol{\nabla}c) = \boldsymbol{\nabla}^2(D_n\, n) + \alpha(c)n, \qquad (1)$$

$$\partial_t c = D_c\boldsymbol{\nabla}^2 c - \beta(c)n. \qquad (2)$$

In Eq. 1, the second term on the left-hand side is the chemotactic drift and the form usually adopted is $\chi(c) = k_1/(k_2 + c)^2$ (16,17). The right-hand side accounts for variations of bacterial density due to diffusion (with diffusivity D_n) and the proliferation term. Various forms are possible for the latter, with general shapes starting at zero for vanishing nutrients and reaching a plateau when nutrients are in excess, e.g., $\alpha(c) = ac^2/(c_*^2 + c^2)$. Results will not depend on this choice. In Eq. 2, the last term is the consumption rate, proportional to the proliferation rate: $\beta(c) = (b/a)\alpha(c)$. Parameters for our experiments are: $D_n \approx 2\times10^{-6}$ cm^2/s; $D_c \approx 6\times10^{-6}$ cm^2/s; $a \approx 6\times10^{-4}$ s^{-1}; and $c_* \approx 2\ \mu$M. As for b, biomass estimates give that each bacterium consumes $\approx$ 200 molecules of glucose/s. A finite carrying capacity of the colony and nonlinear terms in the proliferation rate can be included into the equations above. However, they are immaterial to this analysis, mainly because growth is limited by exhaustion of nutrients in the back of the propagating front, and because, as we shall see in the following, they do not play a role in determining the propagation speed of the front.

Lag phase

Experiments. The initial expansion of a colony inoculated on a dish is slower than the asymptotic one at large times, hence the name, ''lag phase''. To characterize it quantitatively, we first inoculated different quantities of bacteria on NB-rich medium plates and measured the lag time (Fig. 2 *a*). Inocula with fewer bacteria have longer lags, with an increase of roughly 1 h for a 10-fold reduction. (This logarithmic dependency will be rationalized in Appendix B.) We then inoculated several plates with a fixed number of bacteria obtained from various sources, e.g., from the front or the interior of a preexisting moving colony and from liquid cultures in exponential or stationary growth phases. All those cases gave very similar behavior, with colonies from the exponential phase having a lag slightly shorter than the others, yet no major effect was observed.

To test the hypothesis that the lag time might be related to quorum sensing, we prepared the supernatant from a stationary phase culture of *S. typhimurium* and added it to NB plates. Including 100 mM pH 7 MOPS buffer to the plates, we found no differences in the duration of the lag phase between the control plates and plates containing the stationary phase supernatant (an increase of 2 h was observed in the absence of buffer, i.e., letting the pH of the NB medium drop to 6). We conclude that the quorum sensing mechanism is not involved, at least not in the first phase and in our conditions.

To assess the effect of nutrients on the lag period, we prepared plates with nutrients diluted two, four, or eight times or concentrated two or three times. We observed that the poorer the medium, the shorter was the lag phase. To control all components and modify them selectively, we decided to shift to minimal medium plates. We chose medium A as a poor phosphate medium and glucose as carbon source in liquid medium to avoid the impact of high phosphate concentration on motility. We performed a video recording at two different temperatures (23° and 30°C) and with several

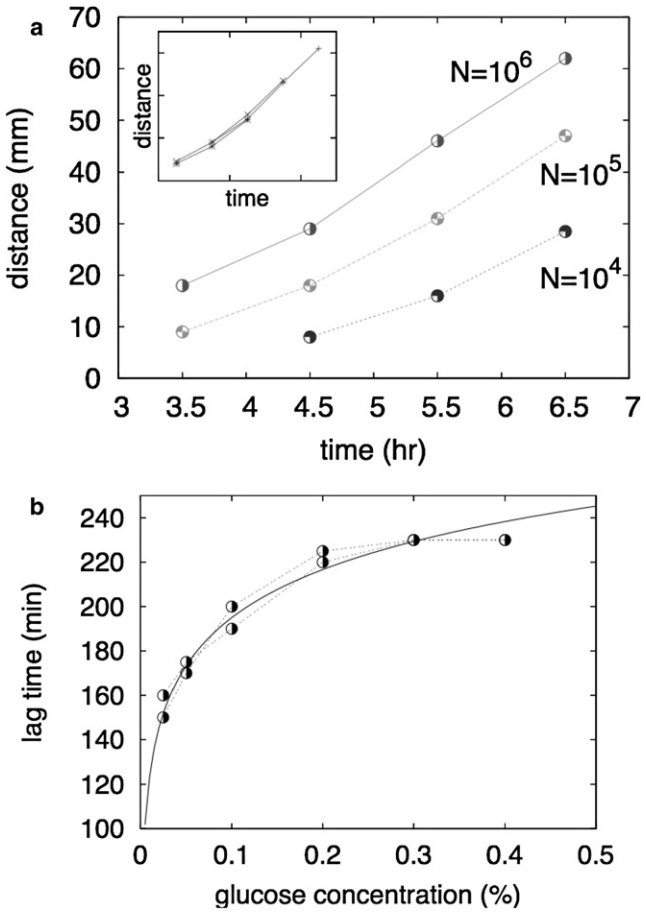

FIGURE 2 Dependency of the lag time on the initial bacterial density and nutrient concentration. (*a*) Distance traveled by the bacterial front in *S. typhimurium* colonies. (*Inset*) Data have been collapsed onto a single curve by a horizontal shift of −1 h (−2 h) for $N = 10^5$ ($N = 10^4$) inoculated bacteria. The 1 h delay per decade agrees with theoretical arguments developed in the text. (*b*) Lag time as a function of glucose concentration for $N = 10^6$ and two independent measurements. The full line is the theoretical prediction.

glucose concentrations (0.025%, 0.05%, 0.1%, 0.2%, 0.3%, and 0.4%; note that a concentration of 0.3% corresponds to $\approx 10^{16}$ molecules in 1 μL). The lag period increases with the nutrient availability, growing from 150 min for 0.025% glucose to >230 min for 0.4% glucose at 30°C (Fig. 2 *b*). At 23°C the lag period is more erratic and goes from 270 min for 0.025% glucose to almost 500 min for 0.3% glucose.

Theory. When bacteria are initially inoculated, the system is generally far from the asymptotic state that dynamically sustains a constant velocity of propagation. In particular, the concentration of nutrients in the interior of the colony is large and the density of bacteria at the front is imposed by the initial condition. The duration of the lag phase is determined by the time taken to go from these initial levels to the asymptotic ones. We show here that the behaviors observed in Fig. 2 *a* are captured by estimating the time needed to bring nutrients within the inoculum to low levels.

Bacteria are inoculated with density n_0 in a medium with uniform nutrient concentration $c_0 \gg c_* \approx 2$ μM. Neglecting diffusion and any saturation in growth, the density follows a simple exponential law $n(t) = n_0 \exp(at)$ and the decrease in the available nutrients follows a complementary law: $c(t) = c_0 - (b/a)n_0[\exp(at) - 1]$. The time taken to bring nutrients inside the inoculum to levels much lower than the initial ones reads $T_{\rm lag} \approx a^{-1} \ln[(a/b)(c_0/n_0)]$, its identification with the lag time $T_{\rm lag}$ anticipating the good comparison with Fig. 2, *a* and *b*. Indeed, the predicted difference in lags between inocula with $N = 10^4$, 10^5, and 10^6 bacteria is $\approx a^{-1}$ ln 10. For a doubling time of 1 30 min, this gives a delay of roughly 1 h. Furthermore, measured lag times are consistent with a logarithmic dependence on glucose concentration, as shown in Fig. 2 *b*. Finally, for an uptake rate $b \approx 200$ molecules cell^{-1} s^{-1}, $N = 10^6$ initial bacteria in 1 μL, and a glucose concentration of 0.3%, the predicted lag is ~4 h, in good agreement with measured values.

Propagation speed

Experiments. After the lag phase, colonies move outwards at a constant speed (see the *inset* in Fig. 2 *a*). At very low (<2 μM) and very high (>20 mM) glucose concentrations, we did not observe any expansion of the colony during the measurement period. In the rich medium (NB) at 37°C, the bacterial front is advancing with speeds reaching 1.6 μm/s (data not shown). In the minimal medium (Fig. 3 *a*), the bacterial speed at 30°C decreased with increasing amounts of glucose (from 0.23 μm/s with 0.025% glucose to 0.13 μm/s with 0.4% glucose). At 23°C, the bacterial speed was smaller and decreased from 0.135 μm/s to 0.085 μm/s.

To understand the cause of the slowdown in Fig. 3 *a* with respect to nutrients, we tracked individual bacteria and measured their velocity distribution. As shown in Fig. 3 *b*, the distribution in the absence of nutrients is Gaussian, yet a metabolic switch takes place after adding glucose. A bimodal distribution ensues: part of the population is swimming at roughly the same velocity but a sizable fraction switches to a slower state.

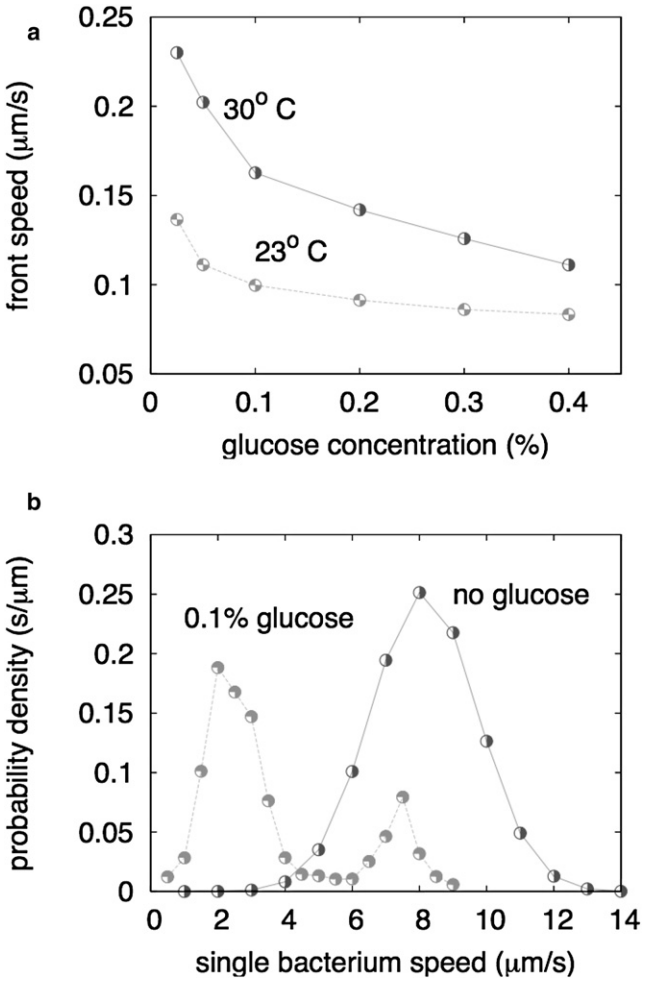

FIGURE 3 The front speed U decreases with glucose concentration. (*a*) U versus glucose concentration at two temperatures. (*b*) Distribution of bacterial speeds before and after (30 min) adding 0.1% glucose. The distribution was obtained by tracking individual bacteria in a dilute population and measuring their speed from their digitized trajectories. Acquisition time was 0.1 s and the vision field was 400 × 400 μm^2.

Theory. Equations 1 and 2 for a single colony and in the absence of chemotaxis admit traveling waves advancing with constant velocity (see (6)). These waves are an example of pulled fronts (see the review by van Saarloos (18)) in that the progression is determined by the region ahead of the front, which is close to the unperturbed initial state. The dynamics of front progression is captured by analyzing the linearized equations. The classical Fisher-Kolmogorov result is that the speed of progression of a radial front expanding from an initially localized inoculum is

$$U_{\rm FK} = 2\sqrt{D_{\rm n}\alpha(c_0)}.$$

It is worth noting that more general forms, including a dependence of the proliferation rate α on n, are possible. Nonetheless, as far as pulled fronts are concerned, such

modifications do not alter the propagation speed, which is determined at the dominant order by the linear dynamics in the limit of vanishingly small bacterial density.

A first remark is that U_{FK} takes values having the same order of magnitude as in Fig. 3 *a*, yet slightly larger. This is relevant as pulled front velocities are a lower bound to the velocity of nonlinear pushed fronts (18), and finite-size corrections (19) are small in our conditions. Nonlinear fronts are then even faster than U_{FK} and this is not easily reconciled with experimental data in Fig. 3 *a*. A second, even stronger remark is that the decrease of the front velocity with increasing nutrients in Fig. 2 *a* cannot be explained. Indeed, the Fisher-Kolmogorov formula gives a constant behavior with respect to the amount of nutrients (assuming they are in excess: $c_0 \gg c_*$). A front velocity decreasing with c would require a decreasing behavior of $\alpha(c)$ versus c, which is quite difficult to justify. Rather, we sought an explanation in terms of the dependence of the bacterial speed on the nutrient concentration. The strongest argument to revise the model is provided by the experiment on the speed distribution in Fig. 3 *b*. Its bimodality suggests a model where bacteria can be in different states of motility and that the respective fractions in the colony are regulated by the nutrients available. The simplest option is to have two states: a slow and a fast mode, characterized by densities n_s and n_f and diffusion coefficients D_s and $D_f > D_s$, respectively. Rates of conversion between the two states are denoted $\gamma_{f\to s}(c)$ and $\gamma_{s\to f}(c)$. The crucial point is that the rates are expected to shift the population toward the slow mode as more nutrients are available. The corresponding equations of motion are

$$\begin{aligned}
\partial_t n_f + \nabla\cdot\left(n_f\chi_f(c)\nabla c\right) &= D_f\nabla^2 n_f + \alpha(c)n_f - \gamma_{f\to s}(c)n_f + \gamma_{s\to f}(c)n_s;\\
\partial_t n_s + \nabla\cdot\left(n_s\chi_s(c)\nabla c\right) &= D_s\nabla^2 n_s + \alpha(c)n_s + \gamma_{f\to s}(c)n_f - \gamma_{s\to f}(c)n_s;\\
\partial_t c &= D_c\nabla^2 c - \beta(c)\left(n_f + n_s\right).
\end{aligned} \tag{3}$$

As described in detail in the Appendices, these equations permit us to account for all of the observed phenomenology. In the absence of chemotaxis we can show analytically that the equations admit a pulled front solution propagating at velocity U, which has both the right magnitude and decreases with increasing nutrients. Since the slow bacteria act as ballast, the velocity U of the pulled front is slowed down as compared to U_{FK}. Furthermore, since the fraction of slow bacteria increases as more nutrients are available, the constancy of U_{FK} is replaced by a net decrease with respect to nutrients available (see Fig. 4 *a*). The same behavior is observed numerically when chemotaxis is present. The pulled front is still the dominant mode for weak chemotaxis while a nonlinear pushed front sets in as chemotaxis gets stronger (see the Supporting Material). Then, the velocity starts to increase with the chemotaxis strength and the density of bacteria is more steeply peaked at the front. We found numerically that the velocity U decreases with nutrients even for strong chemotaxis.

An interesting point worth stressing is the nontrivial distribution of speeds within the bacterial colony. Bacteria of different motility modes are not homogeneously distributed throughout the colony (Fig. 4 *c*). Fast bacteria localize around the edge whereas slow bacteria are dominant in the bulk of the colony. In the region far ahead of the edge, the ratio of the two populations tends to a constant, with a value that can be worked out analytically for the pulled case, without chemotaxis. Note finally that the rates of conversion between the two states of motility that give the curve in Fig. 4 *a* are comparable to the proliferation rates (*inset* of Fig. 4 *c*).

Repulsion or merging?

Experiments. Fig. 1 indicates that merging of subcolonies is predominant for media poor in glucose and at lower agar concentrations, i.e., when bacteria are moving fast. To quantify these observations, we inoculated two sets of plates (0.4% glucose) with different agar concentrations (0.4% and 0.6%) and incubated them for 24 and 66 h, respectively. As shown in Fig. 1, the colonies with 0.4% agar merged, whereas at 0.6% they did not. We then measured the concentration of glucose at various locations on the plate. In the case of overlap, a detectable quantity of glucose is present ahead of the advancing bacterial front (and even within the colonies for some time after their merging). Conversely, the glucose is exhausted in the region between repelling colonies. External regions still contain nutrients and, as the distance to the closest colony increases, their concentration approaches the amount initially present on the plate.

The theoretical analysis below will identify the ratio D_c/U between the rate of diffusion of nutrients and the speed of bacterial fronts as the crucial length-scale. The diffusivity of glucose at 30°C in 0.3% agar minimal medium was measured as $D_c = 6\times10^{-6}$ cm^2/s.

As a limiting case, we also performed experiments with casein, which diffuses very slowly. Using *B. subtilis* protease-producing strain (able to grow on casein as an exclusive source of nutrients), repulsion never occurred in our whole range of agar concentrations (0.3–0.6%), contrary to the glucose-containing medium.

Theory. Far ahead of the colony edge, the bacterial density is small and the consumption term on the right-hand side of the third expression in Eq. 3 is negligible. It follows that the concentration of nutrients differs from the initial concentration

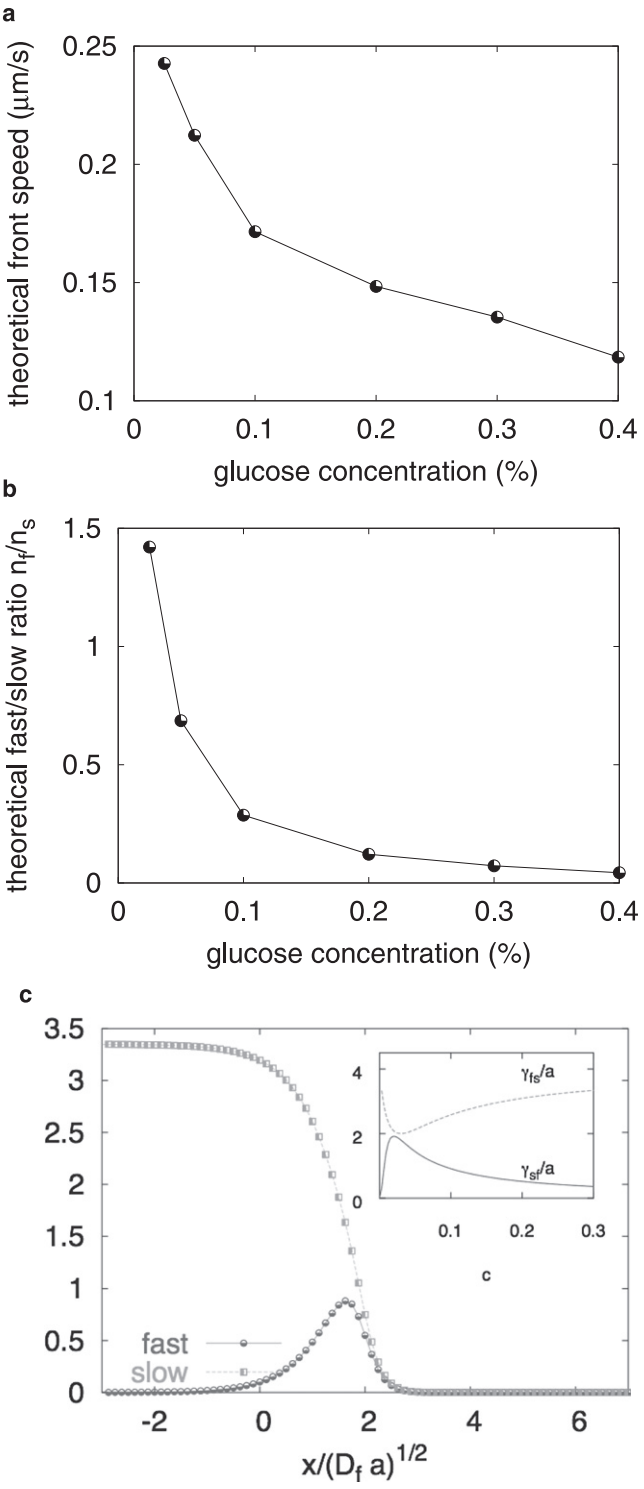

FIGURE 4 (*a*) Selected speed of the bacterial front versus the nutrients available, for the pulled front in the model featuring two states of motility. The ratio $D_s/D_f = 0.0625$, as suggested by Fig. 3. (*b*) The ratio between fast and slow bacterial concentrations in the colony versus the nutrients available. (*c*) Profiles of fast and slow concentrations from numerical simulations at $c = 0.2\%$. (*Inset*) Functional forms of the transition rates adopted in the present simulation.

c_0 by amounts that decrease exponentially as $\exp[-\lambda(r - Ut)]$ with the length-scale $\lambda = D_c/U$. This length-scale (O(1 mm) in our conditions) must be compared to the thickness of the colony edge U/a, ranging from ≈ 1 mm for the fastest fronts to ≈ 150 μm for the slowest ones. For the latter, the bacterial density in the intermediate region is still small, but the nutrient concentration is sizably depleted when subcolonies approach at a distance $\sim\lambda$. If the depletion is strong enough to get nutrients below the threshold of propagation, fronts stop at a finite reciprocal distance. Conversely, fast colonies collide before sensing the other colonies via nutrient depletion. The effect of increased agar concentration observed in Fig. 1 fits the above picture: a denser medium significantly reduces D_n without a comparable alteration of D_c, glucose being a small molecule. As a result, the speed U is reduced, the ratio D_c/D_n is decreased, and repulsion is favored. The absence of repulsion in the experiment on *B. subtilis* with casein is understood similarly by the strong suppression of the ratio D_c/D_n due to the poor motility of casein.

The circular shape of a single colony is strongly perturbed by the presence of approaching one(s) when they get close enough (see Figs. 1 and 5). Analytical arguments described in the Appendices permit us to qualitatively capture the angular dependence of the contours of arrest, as shown in Fig. 5. The remark we exploit is that the aforementioned exponential depletion of nutrients ahead of the colony edge can be captured by a saddle-point argument. In other words, consumption at large times is dominated by regions of the colony, well localized both in space and in time. This is intuitively understood as follows: the consumption due to the most recent past does not have enough time to diffuse far enough, and the far past gives a negligible contribution as the colony was much smaller than its current size. The end-result is a dominant contribution from times slightly

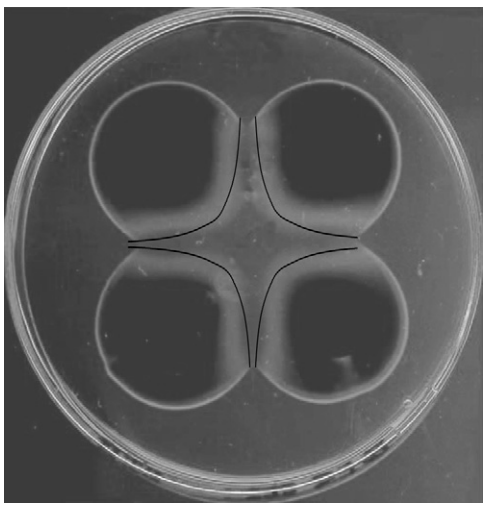

FIGURE 5 The contours of arrest experimentally observed for two and four colonies of *S. typhimurium* and the theoretical prediction superimposed as full lines.

shifted in the past with respect to the current time t. It is then sensible to compute the profile of arrest with the consumption estimated for circular colonies. This reduces the problem to a purely geometrical one, solved explicitly in the Appendices and yielding the prediction in Fig. 5.

DISCUSSION

Collective behaviors of bacterial populations constitute an issue of major biological importance and current interest (20,21). The spreading of colonies on a dish constitutes a setup admittedly simplified, yet already nontrivial. The point we addressed here is the importance of differentiation within the colony and its role in the dynamics of bacterial propagation fronts. The coexistence of bacteria genotypically identical yet differentiated in their physiological motility behavior was directly suggested by the experiments we presented. Regulation of motility with the amount of nutrients is also supported by experiments in batch cultures (22). Differentiation in various functionalities, including motility, was also recently evidenced in biofilm structures of *B. subtilis* (23).

The reaction-diffusion mathematical model that we introduced is not aimed, by its very nature, at capturing the detailed nature of cellular processes. There is no shortage of realistic possibilities, however, that could induce switches in motility. For example, possibilities feature the flagellar clamp mechanism recently discovered by Blair (24), and certain regulatory processes, namely of the production and assembly of flagella. The fact that the transition and reproduction rates that we found are comparable makes it quite likely that dilution of the number of flagella entailed by reproduction is a relevant mechanism. Diversity was introduced in the simplest form, with two possible states of motility, as suggested by the bimodality of our experimental data. A broader scatter of velocities would be more realistic, but this produces no major change and we opted for simplicity. The model indeed captures the experimental phenomenon that was a focus of our attention here, i.e., the slowdown of the propagating colony front as a function of the nutrients available. The slowdown is intuitively understood by the fact that slow bacteria act as ballast, and their fraction increases as more nutrients are available, since more bacteria switch to the less motile state (see Fig. 3 *b*).

As for the second phenomenon discussed here, i.e., the repulsion/merging among subcolonies expanding from different initial inocula, we have demonstrated the major role played by nutrients. We have indeed shown that the parameter controlling the merging or the repulsion of the subcolonies is the ratio between the width of the front and the length D_c/U, built from the nutrient diffusivity and the velocity of the front. For ratios smaller (larger) than unity, repulsion (merging) takes place. For cases of repulsion, the geometry of the contours of the colonies when they arrest is predicted in the Appendices. Screening effects encountered in other geometries of growth are involved in the process. Screening generally refers to the fact that Brownian particles are also unlikely to diffuse to regions that are accessible only via tight entries, e.g., fjords. This is the basic mechanism favoring the formation of irregular dendritic structures. In our setup, screening effects reduce the diffusion of nutrients to the internal region, bounded by the different subcolonies as in Fig. 5, where nutrients eventually become exhausted and fronts, therefore, stop at a finite distance.

In summary, the theoretical and experimental work described here shows that quantitative models for the propagation of fronts in bacterial colonies ought to take into account differentiation within the colony. This is the hallmark of spatially nonuniform structures, namely biofilms, and it is remarkable that the effects of differentiation are so manifest even in the simple geometries considered here. An important direction for future work is a better characterization of the genetic mechanisms at work in the differentiation. Single-cell techniques seem particularly promising to assay, during the development of the colony, and across it, the space-time expression profiles of relevant motility genes.

APPENDIX A: DIFFERENTIATION, SWITCHES IN THE STATE OF MOTILITY, AND THE SPEED OF PROPAGATING FRONTS

We present here the analysis for the velocity of propagation fronts in a model featuring switches between two different states of motility. This is the model proposed in the article, and it accounts for the observed phenomenology. We first present analytical calculations for the pulled front and then discuss the results of numerical simulations for nonlinear fronts. The major point is that the propagation speed of the front decreases quite naturally and generically with nutrients, as observed experimentally.

The equations that describe the evolution of a population with two different states of motility are

$$\begin{aligned}
\partial_t n_f + \nabla\cdot\left(n_f\chi_f(c)\nabla c\right) &= D_f\nabla^2 n_f + \alpha(c)n_f - \gamma_{f\to s}(c)n_f + \gamma_{s\to f}(c)n_s,\\
\partial_t n_s + \nabla\cdot\left(n_s\chi_s(c)\nabla c\right) &= D_s\nabla^2 n_s + \alpha(c)n_s + \gamma_{f\to s}(c)n_f - \gamma_{s\to f}(c)n_s,\\
\partial_t c &= D_c\nabla^2 c - \beta(c)\left(n_f + n_s\right),
\end{aligned} \tag{4}$$

where n_f and n_s are the number density of bacteria in the faster and slower states, respectively.

We shall start by analyzing the behavior of the pulled front, i.e. the equivalent of the Fisher-Kolmogorov traveling wave. To derive the speed of propagation of the pulled front, we consider the region of space far ahead of the front. There, the bacterial densities are very small and this allows the linearization of the above equations around the state $n_f = n_s = 0$, $c = c_0$. At large times the front is approximately planar and it suffices to analyze the case when all the fields depend on a single space coordinate x and time t.

The linearized equations read

$$\begin{aligned}\partial_t n_f &= D_f\nabla^2 n_f + \alpha(c_0)n_f - \gamma_{f\to s}(c_0)n_f + \gamma_{s\to f}(c_0)n_s,\\ \partial_t n_s &= D_s\nabla^2 n_s + \alpha(c_0)n_s + \gamma_{f\to s}(c_0)n_f - \gamma_{s\to f}(c_0)n_s.\end{aligned} \quad (5)$$

Note that the chemotactic terms no longer appear , as they are quadratically small. The equation for the nutrient concentration is not required in the determination of the front speed and is therefore omitted hereafter.

We now investigate the existence of a rightward propagating front and insert the corresponding expressions $n_f(x - Ut)$ and $n_s(x - Ut)$ into the preceding expressions. This results in the following pair of differential equations:

$$\begin{aligned}Un_f' + D_f n_f'' + \alpha(c_0)n_f - \gamma_{f\to s}(c_0)n_f + \gamma_{s\to f}(c_0)n_s &= 0,\\ Un_s' + D_s n_s'' + \alpha(c_0)n_s + \gamma_{f\to s}(c_0)n_f - \gamma_{s\to f}(c_0)n_s &= 0.\end{aligned} \quad (6)$$

The case when proliferation rates vary between the states of motility can be handled similarly. We seek an exponentially decaying solution of the form $n_{f,s}(z) = \hat{n}_{f,s}\exp(-\lambda z)$, which leads to the equations

$$\begin{aligned}-\lambda U\hat{n}_f + \lambda^2 D_f\hat{n}_f + \alpha(c_0)\hat{n}_f - \gamma_{f\to s}(c_0)\hat{n}_f + \gamma_{s\to f}(c_0)\hat{n}_s &= 0,\\ -\lambda U\hat{n}_s + \lambda^2 D_s\hat{n}_s + \alpha(c_0)\hat{n}_s + \gamma_{f\to s}(c_0)\hat{n}_f - \gamma_{s\to f}(c_0)\hat{n}_s &= 0.\end{aligned} \quad (7)$$

It is convenient to adimensionalize the above equations by the transformations

$$\begin{aligned}&\lambda\to\lambda\sqrt{D_f/\alpha(c_0)},\\ &U\to U/\sqrt{D_f\alpha(c_0)},\\ &\gamma\to\gamma/\alpha(c_0),\end{aligned}$$

to obtain

$$\begin{aligned}-\lambda U\hat{n}_f + \lambda^2\hat{n}_f + \hat{n}_f - \gamma_{f\to s}\hat{n}_f + \gamma_{s\to f}\hat{n}_s &= 0,\\ -\lambda U\hat{n}_s + \lambda^2\hat{n}_s\delta + \hat{n}_s + \gamma_{f\to s}\hat{n}_f - \gamma_{s\to f}\hat{n}_s &= 0.\end{aligned} \quad (8)$$

Here, $\delta = D_s/D_f < 1$.

The above system of equations admits a nontrivial solution when its determinant vanishes, i.e., when the following quartic equation is satisfied:

$$\begin{aligned}\left(\lambda^2 - U\lambda + 1 - \gamma_{f\to s}\right)\left(\lambda^2\delta - U\lambda + 1 - \gamma_{s\to f}\right)\\ - \gamma_{f\to s}\gamma_{s\to f} = 0.\end{aligned} \quad (9)$$

Different families of solutions, parameterized by the unknown velocity U, satisfy Eq. 9. The selection of the velocity actually observed for spatially localized initial conditions obey the general heuristics discussed in the review by van Saarloos (18). In particular, for each family of solutions, stable branches should be identified; and the steepness λ, selected in each family, is the largest one. Among different families, the mode selected is the one having the largest velocity, since it is the first to asymptotically invade the unstable region ahead of the front.

To illustrate the selection mechanisms, let us consider first the simplest situation when the conversion from the fast to the slow state is prohibited, i.e., $\gamma_{f\to s} \equiv 0$. Equation 9 factorizes then, and its solutions are $\lambda_{1,2} = (U \pm \sqrt{U^2 - 4})/2$ and $\lambda_{3,4} = (U \pm \sqrt{U^2 - 4\delta(1 - \gamma_{s\to f})})/(2\delta)$. Stability amounts to choosing the branches that give $\lambda \to 0$ when $U \to \infty$, i.e., those with the minus sign in the solutions for λ. The largest steepness λ in each one of the two families is obtained when the discriminant vanishes. The corresponding values of U are $U = 2$ and $U = 2\sqrt{\delta(1 - \gamma_{s\to f})} < 2$. It follows that the selected mode is the former one—i.e., $\lambda = 1$ and $U = 2$—corresponding to the Kolmogorov-Fisher propagation speed of the fast bacteria. This had to be expected as slow bacteria decouple from the fast ones and the calculation was mostly meant to illustrate the methodology to analyze the selection problem in a known case.

A less obvious propagating mode can appear if we consider the case $\gamma_{s\to f} = 0$. Equation 9 factorizes again and its solutions are $\lambda_{1,2} = (U \pm \sqrt{U^2 - 4\delta})/(2\delta)$ and $\lambda_{3,4} = (U \pm \sqrt{U^2 - 4(1 - \gamma_{f\to s})})/2$. The steepnesses of the two stable branches correspond to the vanishing of the discriminants, i.e., $U = 2\sqrt{\delta}$ and $U = 2\sqrt{1 - \gamma_{f\to s}}$. The former corresponds to the Fisher-Kolmogorov mode of slow bacteria, decoupled from the fast ones. Conversely, the latter mode couples fast and slow bacteria, which act as ballast slowing down the progression of the front. The velocity might be rationalized considering that $\alpha(1 - \gamma_{f\to s})$ is the effective proliferation rate of fast bacteria. This velocity is selected if $\delta < 1 - \gamma_{f\to s}$, i.e., $D_s < D_f(1 - \gamma_{f\to s}/\alpha)$.

In the general case when both rates of conversion γ are nonzero, closed expressions are still available for the solutions of the quartic expression (Eq. 9), but they are quite cumbersome. Nevertheless, the same approach as in the previous cases can again be applied to identify the selected mode. This is how we obtained the dependencies shown here in Fig. 6 and extracted the behaviors shown in Fig. 4. The ratio between the diffusivities in the slow and the fast states was set to $\delta \equiv D_s/D_f = 1/16$, the value suggested by experimental data presented in our Fig. 3. Quite intuitively, the velocity of propagation of the front increases if the rate of conversion from the slow to the fast state is accelerated, and vice versa. We further assume that, as clearly indicated by experimental data in Fig. 3, $\gamma_{f\to s}/\gamma_{s\to f}$ is an increasing function of the nutrient concentration. It finally follows that the velocity of the front is a decreasing function of nutrients initially present on the plate as shown in Fig. 4. This property holds quite generally, without any particular need to fine-tune parameters.

The behavior with respect to the strength of the chemotactic drift, i.e., the k_1 in the expression $\chi(c) = k_1/(k_2 + c)^2$, was again obtained by direct numerical simulations using a finite difference scheme. As for the single-state case, below a threshold k_1^*, the pulled front discussed above is the mode selected, while a nonlinear pushed mode sets in above k_1^*. Its velocity increases with k_1 and, most importantly, it generically decreases with nutrients even in the strong nonlinear regime.

APPENDIX B: MODELING THE ARREST OF BACTERIAL FRONTS

In this section we present the quantitative model for the repulsion of bacterial colonies that was described in the body of the article. The concentration of nutrients $c(\boldsymbol{r},t)$ is governed by the equation

$$\partial_t c(\boldsymbol{r},t) = D_c\nabla c(\boldsymbol{r},t) - \eta(\boldsymbol{r},t), \quad (10)$$

where η is the consumption rate field.

Let us consider a single colony growing circularly. For distances from the front much larger that its width, the consumption rate can be treated as a surface term localized at the edge of the colony. This amounts to supposing that the decay length of the bacterial density D_n/U is smaller than the nutrient decay length $\lambda = D_c/U$. As discussed in the article, this condition is met for glucose, where $D_c \simeq 6\times10^{-6}\text{cm}^2/\text{s}$.

For a circular front spreading out with radial velocity U, the consumption reads $\eta(\boldsymbol{r},t) = \sigma\,\delta(r - Ut)$, where we have taken the initial position of the

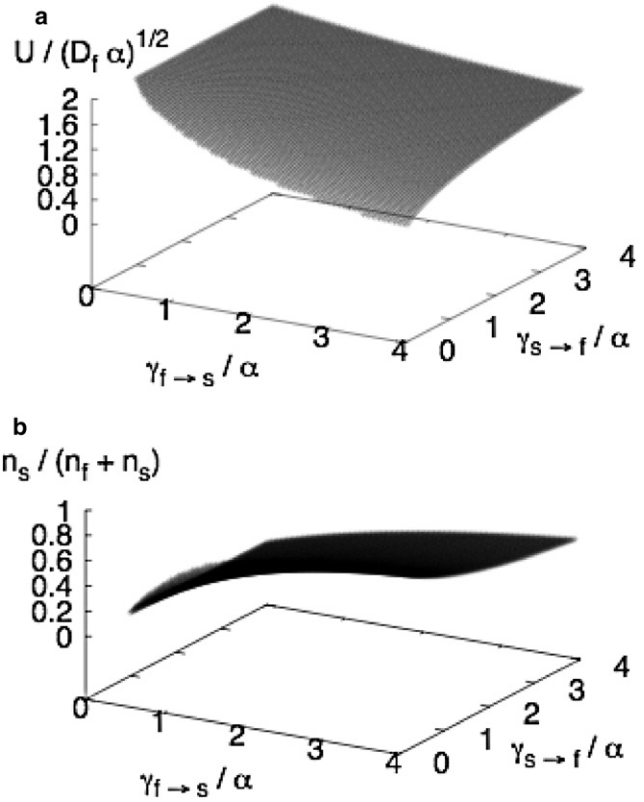

FIGURE 6 Dependencies of the front velocity (*a*) and the fraction of slow bacteria (*b*) versus the conversion rates from fast to slow states of motility and vice versa.

inoculum as the origin of the coordinates and σ is proportional to the width of the front edge, the density of bacteria at the front, and their individual consumption rate. At large times $t \gg D_c/U$, the curvature of the front is weak and the term $(\partial_r c)/r$ in the Laplacian is negligible, compared to the time- and the double space-derivative terms. The resulting expression from Eq. 10 then takes a self-similar form in the variable $z = r - Ut$, the distance to the edge of the colony. The solution decaying at infinity, i.e., representing the consumption due to the colony, is $\propto \exp(-Uz/D_c)$, as already mentioned in the article.

To introduce and motivate the approximations that will follow, we analyze how the previous exponential law builds up. In particular, we want to show that the exponential comes from saddle-point contributions, both in time and in the angle parameterizing the circular profile of the edge of the colony. From Eq. 10, it follows that the depletion of nutrients $d(\boldsymbol{r},t)$ due to the consumption by a circular colony can be expressed via the diffusion kernel as

$$d(\boldsymbol{r},t) \;=\; \int_0^t ds \int d\boldsymbol{w}\, \frac{\eta(\boldsymbol{w},s)}{4\pi D_c (t-s)}\, e^{-\frac{(\boldsymbol{r}-\boldsymbol{w})^2}{4D_c(t-s)}}. \qquad (11)$$

The nutrient concentration c is related to the depletion as $c(\boldsymbol{r},t) = c_0 - d(\boldsymbol{r},t)$. The integral over the angles in Eq. 11 reads

$$\begin{aligned} \textstyle\int_0^{2\pi} d\phi\, e^{\frac{rw\cos\phi}{2D_c(t-s)}} \;&=\; 2\pi I_0\!\left(\tfrac{rw}{2D_c(t-s)}\right) \\ &\simeq\; 2\sqrt{\tfrac{\pi D_c(t-s)}{rw}}\, e^{\frac{rw}{2D_c(t-s)}}, \end{aligned} \qquad (12)$$

where ϕ is the angle between the two vectors $\boldsymbol{r}$ and $\boldsymbol{w}$ and I_0 is the modified Bessel function of order zero. The first equality is the definition of I_0 (formula (3.339) from Gradshteyn and Ryzhik (25)) and the second is the expansion of $I_0(z) \simeq e^z/\sqrt{2\pi z}$ for large values of the argument (formula 8.451.5 from Gradshteyn and Ryzhik (25)).

We observe now that the argument of the exponential in the integrand has a maximum at $\phi = 0$ and rapidly decays around it. The integral is therefore dominated by the contribution coming from a tight region at small angles ϕ, where $rw/D_c(t-s)$ is large. Inserting Eq. 12 into Eq. 11, we obtain

$$d(\boldsymbol{r},t) \;=\; \frac{U^{1/2}\sigma}{\sqrt{4\pi D_c\, r}} \int_0^t \sqrt{\frac{s}{t-s}}\, e^{-\frac{(r-Us)^2}{4D_c(t-s)}}\, ds. \qquad (13)$$

The total distance $r = Ut + z$, where z is the distance to the front.

We are interested in the behavior of Eq. 13 at large times and finite distances z, so that $r \simeq Ut$. To compute Eq. 13, we make the change of variables $x = (t-s)/t$ and observe that the major contribution to the integral comes from a region around the origin of width D_c/U^2t. It is then legitimate to approximate $1 - x$ by unity and extend the region of integration to infinity with exponential accuracy. The integral in Eq. 13 then reduces to

$$d(z)\,1\,\frac{\sigma\sqrt{t}e^{-Uz/2D_c}}{\sqrt{4\pi D_c}} \int_0^\infty \sqrt{\frac{1}{x}}\, e^{-\frac{U^2xt}{4D_c} - \frac{z^2}{4D_c xt}}\, dx \propto e^{-\frac{Uz}{D_c}}. \qquad (14)$$

The second equality follows from the known integral (formula 3.471.15 from Gradshteyn and Ryzhik (19)):

$$\int_0^\infty x^{-1/2} e^{-\gamma x - \beta/x}\, dx \;=\; \sqrt{\pi/\gamma}\, e^{-2\sqrt{\beta\gamma}}.$$

The remark of interest to us is that the value of the integral coincides with the result obtained by the saddle-point method, as can be easily verified by explicit calculation.

Note that the final expression in Eq. 14 coincides with the exponential, which was previously obtained from the asymptotic behavior of the diffusion equation. The arrest of the previous derivation, albeit longer, is that it shows that the consumption is dominated by saddle-point contributions both in the angles and in time. This can be qualitatively understood as follows. On one hand, the far past gives a negligible contribution because the perimeter of the front was much smaller than the current one. On another hand, the consumption due to the most recent times did not have enough time to diffuse up to z. The end-result is a maximum dominant contribution coming from times slightly smaller than the current time t. A similar reasoning accounts for the angular part.

The previous observations on saddle-point dominance demonstrate that the consumption is dominated by contributions around the line connecting the point of arrest to the center of the colony. Furthermore, the dominant contribution at a given time comes from the past, when colonies were much less deformed, possibly still circular. All this suggests the following approximations to compute the shape of the curve where the fronts of the colonies will stop. To simplify things, we shall suppose that the velocity U of the front is a step function of the local nutrient concentration c, i.e., that the velocity vanishes below a threshold K and is equal to a constant U for any concentration $c > K$. This is an approximation, as we know experimentally that the front velocity varies with the nutrient concentration. However, we verified numerically that variations of the order of those observed in Fig. 3 *a* do not affect severely the shape of the stopping profile, as it will also be verified a posteriori.

Nutrients for a single colony reach a time-independent profile after an initial transient. For multiple colonies, the first point of arrest will be reached at t^*, the first time when the consumption due to the other colonies will make the level of nutrients at the front fall below K. The consumption rate $\propto \exp(-Uz/D_c)$ was previously shown to depend on the distance to the front only. It follows that the first point of arrest for two colonies is along the line connecting their centers, and that the profile of arrest for a given colony is symmetric above and below that line. We shall focus on the profile above the line and obtain the lower part by inversion. For times slightly

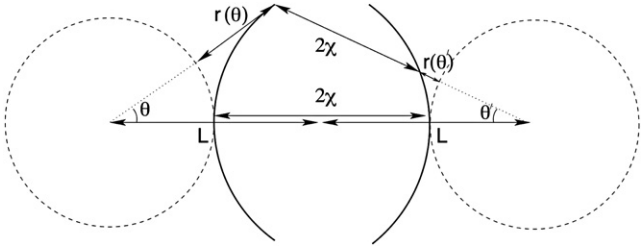

FIGURE 7 Scheme of the geometrical problem involved in the solution of the profile of the bacterial front lines when they halt. The solid lines indicate the profile of arrest for two bacterial colonies. The dotted circles indicate the shape of the colonies at the earliest time of arrest, i.e., at the time of arrest along the line connecting the two centers. We denote the separation between the two colonies at that time by 2χ. This parameter implicitly contains the dependencies on the minimal level of nutrients required for the fronts to move forward, consumption rate, initial nutrient levels, etc. Conservation of the distance 2χ is the nontrivial condition that we impose to compute the shape of the line of arrest of the fronts. In other words, along the direction connecting the point of arrest at time t to the center of the other colony, the distance to the other front should remain equal to 2χ at all t-values. This condition is justified in the body of the text by analyzing the dynamics of nutrient consumption and its saddle-point nature.

larger than t^*, the point of arrest will start moving upwards, at larger θ-values. Previous arguments on saddle-point dominance indicate that it is a sensible approximation to compute the line of arrest as the locus of points such that their distance to the facing colony along the line connecting to its center remains constant as time progresses.

The problem is then reduced to simple geometry, as sketched in Fig. 7. Denoting by $2L$ the initial distance between the two inocula and 2χ the distance between the first two points of arrest, the distance from the center of a colony to its point of arrest at the angle θ is defined as $L - \chi + r(\theta)$, where $r(0) = 0$. The unknown function $r(\theta)$ is obtained from the two equations

$$\begin{aligned}(L + r(\theta') + \chi)\sin\theta' &= (L - \chi + r(\theta))\sin\theta \\ (L + r(\theta') + \chi)\cos\theta' &+ (L - \chi + r(\theta))\cos\theta = 2L,\end{aligned} \tag{15}$$

immediately following from Fig. 7.

The expressions in Eq. 15 have a simple solution at small angles θ,

$$\theta \simeq \theta'\frac{L+\chi}{L-\chi}; \quad r(\theta') \simeq \frac{L}{2}\frac{L^2-\chi^2}{L^2+\chi^2}\theta'^2, \tag{16}$$

simply obtained by Taylor expanding the various quantities. Similarly, when $\cos\theta' << 1$, we obtain

$$\theta \simeq \theta' + \frac{2\chi}{L}\sin\theta'\cos^2\theta', \tag{17}$$

$$r(\theta') \simeq \frac{L}{\cos\theta'} - L - \frac{\chi^2\sin^2\theta'}{L}\cos\theta' + \frac{5}{2}\frac{\chi^3\sin^4\theta'}{L^2}\cos^2\theta'. \tag{18}$$

For intermediate values of the angles, we found the behavior of the curve $r(\theta)$ solving the expressions in Eq. 15 iteratively. In the iterations, we move progressively from small angles to larger ones and, for each θ, we solve the first equation to find $\theta'(\theta)$ and use the value of $r(\theta')$ (which is already computed as $\theta \geq \theta'$) to compute $r(\theta)$. The scheme is initiated at very small angles using the expansion from Eq. 16.

For more than two inocula, the reasoning is similar, except that Eq. 14 is modified to a sum of contributions from the other colonies. Identifying numerically the locus of points where depletion makes the nutrients fall below the threshold of motility yields the curve shown in Fig. 5. Note the shrinking of the distance between the two fronts, which has the effect of preventing replenishment of nutrients in the intercolony region from the outside, where concentration of nutrients is still high. This screening effect is because particles of nutrients random-walking towards the interior will be likely to touch the fronts and be absorbed.

SUPPORTING MATERIAL

One figure is available at http://www.biophysj.org/biophysj/supplemental/S0006-3495(09)00795-4.

The work was supported by ANR 07 NANO grant No. 062 03.

REFERENCES

1. Fujikawa, H., and M. J. Matsushita. 1989. Fractal growth of *Bacillus subtilis* on agar plates. *J. Phys. Soc. Jpn.* 58:3875–3878.
2. Czirok, A., E. Ben-Jacob, I. Cohen, and T. Vicsek. 1996. Formation of complex bacterial colonies via self-generated vortices. *Phys. Rev. E Stat. Phys. Plasmas Fluids Relat. Interdiscip. Topics.* 54: 1791–1801.
3. Ben-Jacob, E., I. Cohen, and H. Levine. 2000. Cooperative self-organization of microorganisms. *Adv. Phys.* 49:395–554.
4. Wu, Y., Y. Jiang, D. Kaiser, and M. Alber. 2007. Social interactions in myxobacterial swarming. *PLoS Comp. Biol.* 3:12:e253.
5. Adler, J. 1966. Chemotaxis in bacteria. *Science.* 153:708–716.
6. Murray, J. D. 2002. Mathematical Biology, 3rd Ed. Springer Verlag, Berlin, Germany.
7. Brenner, M. P., L. Levitov, and E. Budrene. 1998. Physical mechanisms for chemotactic pattern formation by bacteria. *Biophys. J.* 74:1677–1693.
8. Budrene, E., and H. C. Berg. 1995. Dynamics of formation of symmetrical patterns by chemotactic bacteria. *Nature.* 376:49–53.
9. Adler, J., Q. L. Hazelbauer, and M. M. Dahl. 1973. Chemotaxis toward sugars in *Escherichia coli*. *J. Bacteriol.* 115:824–847.
10. McClelland, M. 2001. Complete genome sequence of *Salmonella enterica* serovar *Typhimurium* LT2. *Nature.* 413:852–856.
11. Blattner, F. R. 1997. The complete genome sequence of *Escherichia coli* K-12. *Science.* 277:1453–1474.
12. Medigue, C. 2005. Coping with cold: the genome of the versatile marine Antarctica bacterium *Pseudoalteromonas haloplanktis* TAC125. *Genome Res.* 15:1325–1335.
13. Spizizen, J. 1958. Transformation of biochemically deficient strains of *Bacillus subtilis* by deoxyribonucleate. *Proc. Natl. Acad. Sci. USA.* 44:1072–1078.
14. Neidhardt, F. C. 1974. Culture medium for enterobacteria. *J. Bacteriol.* 119:736–747.
15. Bozal, N. 1997. *Pseudoalteromonas antarctica* sp. nov., isolated from an Antarctic coastal environment. *Int. J. Syst. Bacteriol.* 47:345–351.
16. Lapidus, I. R., and R. Schiller. 1976. Model for chemotactic response of a bacterial population. *Biophys. J.* 16:779–789.
17. Block, S. M., J. E. Segall, and H. C. Berg. 1982. Impulse responses in bacterial chemotaxis. *Cell.* 31:215–226.
18. van Saarloos, W. 2003. Front propagation into unstable states. *Phys. Rep.* 386:29–222.
19. Brunet, E., and B. Derrida. 1997. Shift in the velocity of a front due to a cutoff. *Phys. Rev. E Stat. Phys. Plasmas Fluids Relat. Interdiscip. Topics.* 56:2597–2604.

20. Ackermann, M. 2008. Self-destructive cooperation mediated by phenotypic noise. *Nature*. 454:987–990.

21. Gibbs, K. A., M. L. Urbanowski, and E. P. Greenberg. 2008. Genetic determinants of self-identity and social recognition in bacteria. *Science*. 321:256–259.

22. Amsler, C. D., M. Cho, and P. Matsumure. 1993. Multiple factors underlying the maximum motility of *E. coli* as cultures enter post-exponential growth. *J. Bacteriol*. 175:6238–6244.

23. Vlamakis, H., S. Aguilar, R. Losick, and R. Kolter. 2008. Control of cell fate by formation of an architecturally complex bacterial community. *Genes Dev*. 22:945–953.

24. Blair, K. M. 2008. A molecular clutch disables flagella in the *Bacillus subtilis* biofilm. *Science*. 320:1636–1638.

25. Gradshteyn, I. S., and I. M. Ryzhik. 2000. Table of Integrals, Series and Products, 6th ed. Academic Press, New York.